ARTICLE TYPE www. rsc.org/xxxxxx | XXXXXXXX

Reduction Mechanisms of the CuO(111) surface through surface oxygen vacancy formation and hydrogen adsorption†

Yasheng Maimaiti,[a] Michael Nolan,[a] Simon D Elliott*[a]

Received Xth XXXXXXXXXX 20XX, Accepted Xth XXXXXXXXX 20XX

First published on the web Xth XXXXXXXXXX 200X

DOI: 10.1039/b000000x

We studied the reduction of CuO(111) surface using density functional theory (DFT) with the generalized gradient approximation corrected for on-site Coulomb interactions (GGA+U) and screened hybrid DFT (HSE06 functional). The surface reduction process by oxygen vacancy formation and H_2 adsorption on the CuO(111) surface is investigated as two different reduction mechanisms. We found that four coordinated subsurface oxygen O(u) is more thermodynamically favourable than the three coordinated surface oxygen O(3) by 0.34 (GGA + U) and 0.48 eV (HSE06). It is also found that both GGA + U and HSE06 predict the same trend in the relative stability of surface and subsurface oxygen vacancies with (2 × 1) slab. Cu^+ ions are formed upon the removal of one oxygen atom per cell. At $\Theta = \frac{1}{4}$ vacancy concentration,the subsurface oxygen vacancy pair $V_{O(u)}$ + $V_{O(d)}$ is found to be energetically most favourable among all the possible vacancy pairs in the subsurface and the surface. The reduction of Cu^{2+} to Cu^+ is found to be more favourable than that of Cu^+ to Cu^0 in the most stable vacancy structures at all concentrations. As the oxygen vacancy concentration increases, mixture of subsurface and surface vacancies is energetically preferred over full reduction of the surface or subsurface monolayer. Consistent with the oxygen vacancy calculations, H_2 adsorption occurrs initially on the O(3) atom but not on O(4). Water molecules are formed upon the adsorption of H_2 and thus reduce the CuO(111) surface to metallic Cu. *Ab initio* atomistic thermodynamics shows that reducing CuO to metallic Cu at the surface is more energetically difficult than in the bulk. Using H_2 as the reducing agent, it is found that the CuO surface is reduced to Cu_2O approximately at 360 K and that complete reduction from Cu_2O to metallic Cu occurs at 780 K.

1 Introduction

Copper is the main interconnect material for microelectronics applications because of its low resistivity and high stability against electromigration.[1] A process to deposit a uniform and continuous thin film (< 2 nm) of copper in high aspect ratio structures is desirable in order to meet the demands of current trends in integrated circuit technology. Deposition techniques including physical vapour deposition (PVD),[2] electrodeposition,[3] chemical vapour deposition (CVD),[4] and atomic layer

† Electronic Supplementary Information (ESI) available: Optimized structures of multiple oxygen vacancies on the CuO(111) surface are given in ESI. See DOI: 10.1039/b000000x/

[a] *Tyndall National Institute, University College Cork, Lee Maltings, Prospect Row, Cork, Ireland. E-mail: simon.elliott@tyndall.ie*

deposition (ALD)[5] have been applied with the aim of obtaining such a thin film. However, it is extremely difficult to deposit thin films of Cu at this thickness and instead islands of Cu tend to be more favourable.[6] Of these deposition approaches, ALD shows the most promise in surmounting the island growth problem as well as meeting future demands of device scaling.

The reactions of copper (I) and copper (II) compounds with H_2 have been reported as a way to achieve copper metal ALD.[5,7] Unfortunately, the typical temperature requirement for these reactions (200–400 °C) causes dewetting which leads to discontinuous copper films. Recently, Sung *et al.* reported thermal ALD of copper metal using the reaction of copper dimethylamino-2-propoxide [$Cu(dmap)_2$] and diethylzinc [$ZnEt_2$] at 100–120 °C.[5] However, subsequent work reported that the parasitic chemical vapour deposition reaction of $ZnEt_2$ may lead to Zn incorporation into the copper thin film.[6] Plasma-enhanced ALD is considered to be a less suitable approach to deposit metal thin films on substrates with high-aspect-ratios because the plasma recombines at metallic surfaces and becomes inactive within deep features.[8]

On the other hand, ALD of many metal oxides and nitrides is successful and the reaction mechanism is quite well understood.[9] For this reason, indirect approaches for metal ALD from oxides and nitrides based on the reduction of the corresponding oxide/nitride have been proposed.[10] This type of metal ALD is characterized by two steps: ALD of the metal oxide or nitride and reduction to the metal with a reducing agent. Examples of this indirect approach to metal ALD include ALD of Cu_3N followed by reduction to Cu metal by treatment with H_2 at 160 °C[11] and ALD of CuO followed by reduction to Cu metal with H_2 at 270–320 °C.[10] More recently, Knisley *et al.* reported low temperature deposition of high purity copper film through ALD of copper (II) formate, which is then readily reduced to Cu metal by a hydrazine (N_2H_4) pulse at 80 °C.[12] Cu islands and discontinuous thin films on the substrate are observed in these indirect ALD methods after the reduction to metallic Cu. The indirect ALD has also been applied to deposit other metals. The atomic layer of NiO is reduced to Ni metal after ALD process using H_2 radical at 165 °C.[13] The Ir metal is obtained from reducing IrO_2 by applying H_2 pulse at 120–180 °C after each ALD cycle of IrO_2.[14] Ideally, the reduction process that follows ALD should be carefully chosen so as to obtain conformal and uniform thin metal films at low temperature, but it is not clear whether it is possible. Experimentally, metal oxides have been reduced to corresponding metal using different methods. Lee *et al.* reduced CuO to metallic copper through vacuum annealing at 673 K.[30] Kim *et al.* reported CuO reduction at atmospheric pressure of H_2 and temperatures of 423-573 K.[37,38] Reduction of NiO with H_2 was studied by Rodriguez and co-workers using *in situ* time-resolved XRD and NEXAFS/EXAFS at atmospheric pressure of H_2 and temperatures of 523-623 K.[39]. In advancing Cu film growth, it is necessary to understand the reduction mechanisms of metal oxides to the corresponding metal.

In this paper, we study the reduction of a CuO surface (that would be grown with ALD) to metallic Cu using density functional theory (DFT) with the generalized gradient approximation (GGA) corrected for on-site Coulomb interactions through the Hubbard U correction (GGA+U) and screened hybrid density functional (HSE06).[21,22] The CuO(111) surface is

the most stable, as measured by surface energy, and hence we consider only this surface for our study (sect. 3). Two possible mechanisms for CuO reduction to metallic Cu are studied: direct formation of oxygen vacancies by removal of neutral oxygen from surface and subsurface as the model of vacuum annealing method in Ref. 30 (sect. 4) and the reaction of H_2 with oxygen on the CuO(111) surface to form water as the model of reduction of CuO with reducing agent H_2 in Refs. 37,38 (sect. 5). Using *Ab initio* atomistic thermodynamics, we relate our computational results with these two different reduction methods, and we get new insight into how CuO surface is reduced to metallic Cu.

2 Computational Methods

All calculations were performed using DFT implemented in the VASP code,[15] in which the valence electron states are expanded in a plane-wave basis set with an energy cutoff of 400 eV.[16] Exchange and correlation are treated within the generalized gradient approximation (GGA), using the Perdew-Burke-Ernzerhof (PBE) functional.[17] Since conventional DFT functionals are unable to describe the strong correlation effect among the partially filled Cu 3d states in CuO,[18] the Hubbard parameter, U, is introduced for the Cu 3d electrons to describe the on-site Coulomb interaction, giving the well-known GGA+U method.[19] The values of U = 7 eV and J = 0 eV for CuO were adopted from Ref 20. In sect. 4, we discuss the effect of U. Spin polarized calculations were performed since bulk CuO has an antiferromagnetic ground state. For bulk CuO, an $8 \times 8 \times 8$ k-point grid within the Monkhorst-Pack scheme in the Brillioun zone was employed. To allow the vacancy formation energy and adsorption energy to be obtained, gas phase H_2, O_2 and H_2O molecules were calculated in the CuO(111)–(2×1) supercell without CuO. Full geometry relaxation of all surface structures was carried out using the conjugate gradient method for energy minimization until the forces on each ion were less than 0.02 eV/Å.

To study oxygen vacancy formation and H_2 adsorption on CuO(111) surface, a (2×1) surface supercell expansion was used and a (2×2) surface supercell was also used to check the results for oxygen vacancy formation. The slab thickness was six layers (12.4 Å), with a 15 Å vacuum gap. The Brillouin zone was sampled with a $4 \times 8 \times 1$ k-point grid. For the oxygen vacancy calculations, we validate our results by using the Heyd–Scuseria–Ernzerhof (HSE06) hybrid functional with the exchange screening length of 0.2 $Å^{-1}$, where correlation is described in GGA (PBE) and the exchange is a mixture of 25% exact (HF) exchange and 75% PBE exchange.[21,22] A $2 \times 4 \times 1$ k-point grid is used for all the HSE06 calculations due to the computational intensity of the hybrid functional.

The formation energy per oxygen vacancy is defined as

$$E_{\mathrm{vac}} = E(\mathrm{CuO}_{1-n\delta}) - E(\mathrm{CuO}_{1-(n-1)\delta}) + \frac{1}{2}E(\mathrm{O}_2) \qquad (1)$$

where $E(\mathrm{CuO}_{1-n\delta})$ and $E(\mathrm{CuO}_{1-(n-1)\delta})$ are the energies of the slabs with n and $n-1$ number of oxygen vacancies, respectively. Here, positive number is a cost. δ is the vacancy concentration that results from removing one oxygen atom from the cell. In our (2×1) slab, $\delta = 0.25$ for one oxygen vacancy in a layer. $E(\mathrm{O}_2)$ is the energy of oxygen molecule in the gas phase and corresponds to the chemical potential of oxygen gas at standard pressure and T=0 K. While the GGA method overbinds the O_2 molecule by 0.7 eV per atom relative to the

experiment,[23] which leads to overstabilisation of an oxygen vacancy, the trends in oxygen vacancy stability are expected to be unaffected by this constant error. The HSE06 functional has been used by Ganduglia-Pirovano *et al* for studying oxygen vacancies in the CeO_2 surface, where they found that DFT + U and HSE06 predict the relative stability correctly.[24] Thus, the overstabilisation of oxygen vacancies in our calculations can be assessed by using HSE06.

For the adsorption of H_2 onto the CuO(111) surface, the adsorption energy ΔE_{ads} is calculated from:

$$\Delta E_{\text{ads}} = E(\text{H}_2@\text{CuO}_{1-n\delta}) - E(\text{CuO}_{1-n\delta}) - E(\text{H}_2) \quad (2)$$

where $E(\text{H}_2@\text{CuO}_{1-n\delta})$ is the energy of CuO(111) surface with n oxygen vacancies and a H_2 molecule adsorbed. $E(\text{H}_2)$ is the energy of a hydrogen molecule in the gas phase and thus represents conditions of $P_{\text{H}_2} = 1$ atm and $T = 0$ K.

The desorption energy of a water molecule from the partially reduced CuO (111) surface after H_2 adsorption is calculated from:

$$\Delta E_{\text{des}} = E(\text{CuO}_{1-(n-1)\delta}) + E(\text{H}_2\text{O}) - E(\text{H}_2@\text{CuO}_{1-n\delta}) \quad (3)$$

where $E(\text{H}_2\text{O})$ is the energy of a water molecule in the gas phase. If the desorption energy is negative, desorption of the water molecule into the vacuum is favourable. The reduction energy E_{red} of the CuO (111) surface with H_2 is thus defined as the sum of adsorption and desorption energies above:

$$E_{\text{red}} = E_{\text{ads}} + E_{\text{des}} \quad (4)$$

In order to investigate the surface stability across a range of experimental conditions, we apply *ab initio* thermodynamics[25] to the two cases of CuO(111) surface reduction – oxygen vacancy formation and H_2 adsorption on the CuO(111) surface. At temperature T, and pressure P, the surface free energy of the CuO(111) surface can be defined

$$\gamma(T,P) = \frac{1}{A}[G - \sum_i N_i \mu_i(T,P)] \quad (5)$$

where G is the Gibbs free energy of the solid with the surface area A. $\mu_i(T,P)$ is the chemical potential of the ith species and N_i is the number of units in the system. In the first case, for vacuum annealing of CuO (sect. 4), only two atom types are present and react according to the stoichiometry Cu + O→ CuO so that $\mu_{\text{Cu}} + \mu_{\text{O}} = \mu_{\text{CuO}}$. Hence Eq. (5) can be written as a function of one chemical potential:

$$\begin{aligned} \gamma(T,P) &= \frac{1}{A}[E_{\text{slab}} - N_{\text{Cu}}\mu_{\text{Cu}} - N_{\text{O}}\mu_{\text{O}}] \\ &= \frac{1}{A}[E_{\text{slab}} - N_{\text{Cu}}\mu_{\text{CuO}} + N_{\text{vac}}\mu_{\text{O}}] \end{aligned} \quad (6)$$

where $N_{\text{vac}} = N_{\text{Cu}} - N_{\text{O}}$ is the number of oxygen vacancies on the CuO(111) surface, and the plus sign means an oxygen deficiency in the system. The oxygen chemical potential μ_{O} can be related to the oxygen pressure P and the temperature T by

$$\mu_{\text{O}}(T,P) = \mu(T,P^0) + \frac{1}{2}kT \ln \frac{P}{P^0} \quad (7)$$

To determine the range of the oxygen chemical potential, we set the maximum value of $\mu_{\text{O}}(T,P)$ to be the total energy of oxygen in the gas phase, i. e., $\mu_{\text{O}}(0,P^0) = \frac{1}{2}E(\text{O}_2) = 0$, which corresponds to the oxygen-rich condition. The minimum of $\mu_{\text{O}}(T,P)$ can be defined as the condition where bulk CuO transforms to Cu bulk and releases oxygen and this corre-

sponds to the oxygen-poor condition. Thus, the allowed range of μ_O is

$$\mu_{CuO} - \mu_{Cu} < \mu_O < \frac{1}{2}E(O_2) \quad (8)$$

From this we can obtain the allowed range for the change in μ_O, which is

$$h_{CuO} < \Delta\mu < 0 \quad (9)$$

where $h_{CuO} = E^{bulk}_{CuO} - E^{bulk}_{Cu} - \frac{1}{2}E(O_2)$, denotes the formation energy of bulk CuO, and where $\Delta\mu_O = \mu_O - \frac{1}{2}E(O_2)$.
In the second case, we consider the effect of a chemical reducing agent, namely H_2 gas (sect. 5). In principle this introduces an additional variable μ_{H_2}. However, given that $H_2 + \frac{1}{2}O_2 \rightarrow H_2O$, it is experimentally reasonable to set $\mu_{H_2O} = E(H_2O)$ as constant and restrict our focus to the oxygen poor condition $\mu_O \leq \mu_{CuO} - \mu_{Cu}$. Now the single variable μ_{H_2} can range between $\mu_{H_2} = E(H_2)$ and $\mu_{H_2} = \mu_{H_2O} - \mu_O = E(H_2O) - \mu_{CuO} + \mu_{Cu}$. Hence, μ_O is given by

$$\mu_O = \mu_{H_2O} - \mu_{H_2} \quad (10)$$

and the available range of oxygen chemical potential μ_O is taken as follows,

$$\mu_{H_2O} - \mu_{H_2} < \mu_O < \mu_{CuO} - \mu_{Cu} \quad (11)$$

This indicates that the minimum value of μ_O during the reduction of CuO via oxygen vacancies (eq. (9)) is the maximum value of μ_O during the reduction of CuO surface with H_2 adsorption.

3 CuO(111) surface

To check the applicability and accuracy of the GGA+U approach with the chosen parameters, we first performed calculations to optimize the structural parameters of bulk CuO. The calculated lattice parameters are **a**=4.683 Å, **b**=3.43 Å, **c**=5.138 Å, β=99.2° and the Cu–O distance is 1.95 Å, in good agreement with experimental data.[26] Fig. 1(a) shows the bulk structure and antiferromagnetic spin ordering in bulk CuO. Fig. 2 shows the total electronic density of states (DOS) and the DOS projected on Cu and O states in bulk CuO. The GGA+U band gap is about 1.3 eV which is underestimated compared to experiment (1.9 eV)[27] and consistent with an earlier calculation (1.1 eV).[28] The calculated magnetic moment per Cu atom is 0.63 μ_B, which is consistent with experiment (0.68 μ_B).[29] This indicates that the GGA+U approach with chosen U and J is appropriate for describing antiferromagnetic bulk CuO.

To identify the most stable surface of CuO, several different low index surfaces are studied. Surface energies for these surfaces are calculated with the formula $\gamma_{surf} = ((E_{slab} - nE_{bulk}))/2A$, where E_{slab} is the energy of stoichiometric CuO, E_{bulk} is the CuO bulk energy and A is the surface area. The factor of 2 comes from the two slab surfaces. The computed surface energies are 0.72, 0.91, 1.18, 1.68 and 2.24 J/m^2 for CuO(111), CuO(011), CuO(110), CuO(010) and CuO(100) stoichiometric surfaces, respectively. This indicates that the CuO(111) surface is the most stable compared to other stoichiometric surfaces, which is consistent with the report by Hu *et al.*[28] The surface energies of nonstoichiometric surfaces including O- and Cu- terminated CuO(110) and CuO(100) are evaluated as the function of μ_O, and it is found that these non-

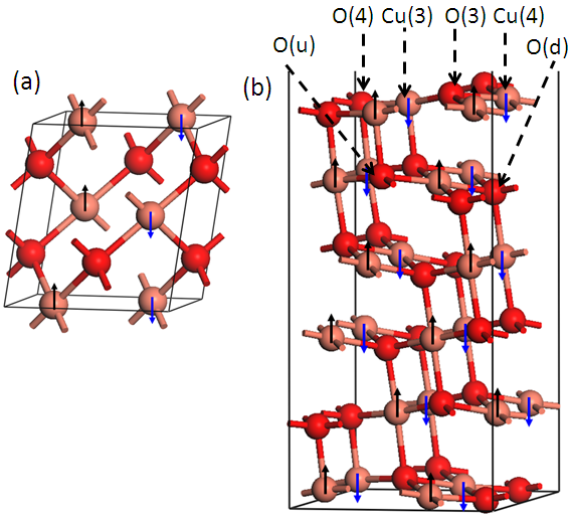

Fig. 1 Structure and antiferromagnetic spin ordering of (a) CuO bulk. (b) CuO(111) slab. The red and salmon pink balls represent oxygen and copper atoms, respectively and this colour scheme is used throughout the paper. Arrows in black represent spin up states and arrows in blue represent spin down states. Four coordinated Cu and O atoms on the surface are labelled Cu(4) and O(4), while three coordinated Cu and O atoms are labelled Cu(3) and O(3), respectively. The subsurface oxygen atoms which coordinated with three Cu atoms on the subsurface and one Cu atom on the surface are labeled O(u); The subsurface oxygen atoms which coordinated with three Cu atoms on the subsurface and one Cu atom on the subsubsurface are labeled O(d).

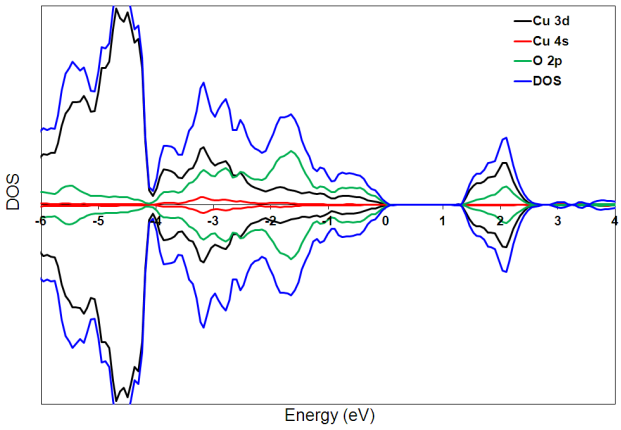

Fig. 2 Total electronic density of states (DOS) and projection of the DOS onto Cu 3d and 4s and O 2p states of CuO bulk. The top of the valence band is aligned to 0 eV.

stoichiometric surfaces are even more stable than CuO(111) surface in a narrow range near the limit of O–rich condition which is difficult to achieve in typical experimental condition.[28] Thus we choose the CuO(111) surface as a model surface to study the reduction process of the CuO. For the CuO(111) surface calculation, we find that a bulk-like magnetic ordering is the most stable, which is depicted by arrows on the Cu atoms of the relaxed structure of the stoichiometric CuO(111) shown in Fig. 1(b). The other possibilities of magnetic ordering were studied in detail in the paper by Hu *et al.*[28] The CuO(111) surface has two kinds of geometrically different oxygen atoms (Fig. 1(b)): those that are coordinated with three Cu atoms on the surface and one Cu atom on the subsurface, denoted O(4), and those which are only coordinated with three surface Cu atoms, denoted O(3). O(3) atoms are more exposed on the surface compared to O(4). The four coordinated Cu atoms, denoted Cu(4), are coordinated to four oxygen atoms within the plane of the surface. All the oxygen atoms on the subsurface are four coordinated, which bonds with the three Cu atoms on the plane, and one with either surface Cu atom or subsubsurface Cu atom, which are denoted O(u) and O(d). Three-fold Cu atoms, denoted Cu(3), are coordinated with O(3) and O(4) atoms on the surface and one O(3) atom of the subsurface. The distinction between O(3), O(4), O(u) and O(d) ions is important, as they behave very differently during the reduction of the CuO(111) surface.

4 Oxygen vacancies on CuO(111) surface

Removing neutral oxygen atoms so as to create oxygen vacancies is the simplest way to investigate how CuO can be reduced to metallic copper. The magnitude of the oxygen vacancy formation energy plays a crucial role in this process:

if the formation energy of oxygen vacancies is too high then desorption of oxygen into vacuum will not be favourable. To this end, we consider different coverages (Θ) of surface, subsurface and a mixture of surface/subsurface oxygen vacancies on a (2×1) surface supercell of the CuO(111) surface. This gives insight into the energetics of formation of metallic copper during the reduction process. In the following subsection, we discuss each coverage in turn – ranging from $\Theta = \frac{1}{4}$ oxygen vacancies (removal of one oxygen per cell) to $\Theta = 1$ oxygen vacancies at the surface (removal of four oxygen per cell).

4.1 $\Theta = \frac{1}{4}$ Oxygen Vacancy

Since there are two types of oxygen atoms in the surface/subsurface of CuO(111), we consider two types of oxygen vacancy each for surface and subsurface. namely, $V_{O(3)}$ and $V_{O(4)}$ on the surface by removing three-fold O(3) and four-fold O(4) coordinated surface oxygen atoms, and $V_{O(u)}$ and $V_{O(d)}$ on the subsurface by removing up-bonded O(u) and down-bonded O(d) oxygen atoms (See Fig. 1b). The oxygen vacancy formation energies are calculated using Eq. 1, and are listed from left to right in Table 1 according to the energetic preference. We can see that both DFT + U and HSE06 predict that the structure with subsurface $V_{O(u)}$ vacancy is energetically more favourable than the structure with surface $V_{O(3)}$ vacancy by 0.34 (GGA + U) and 0.48 eV (HSE06). The preference for subsurface oxygen vacancy over the surface oxygen vacancy was also found for $CeO_2(111)$.[24] The second most stable structure is the structure with $V_{O(3)}$ vacancy has a computed formation energy of 3.02 eV by GGA + U and 2.77 eV by HSE06, which is energetically more favourable than the structure with $V_{O(4)}$ vacancy, which has a formation energy of 3.52 eV by GGA + U and 3.27 eV by HSE06. This is not surprising because O(3) is under-coordinated. While GGA + U produces same formation energies of 3.52 eV for $V_{O(4)}$ and $V_{O(d)}$ vacancies, HSE06 predicts that $V_{O(d)}$ has the slightly smaller formation energy than $V_{O(4)}$. The magnitude of the vacancy formation energy indicates that the stoichiometric CuO(111) surface is quite stable under conditions of high O_2 pressure, where $\mu_{O_2} = E(O_2)$. Nevertheless, a comparison of the computed energies with those of well-known reducible metal oxide surfaces such as $CeO_2(111)$[32] and $TiO_2(110)$[24], indicates that the CuO(111) surface can be classed as reducible.

To check size effects in the surface supercell, we also calculated E_{vac} in a (2×2) supercell expansion using GGA + U. The calculated E_{vac} is 2.91 eV for $V_{O(3)}$ and 3.16 eV for $V_{O(4)}$ on the (2×2)–CuO(111) surface with $\Theta = \frac{1}{8}$ oxygen vacancy. A (2×2)–CuO(111) surface with a $\Theta = \frac{1}{4}$ oxygen vacancy concentration has E_{vac} of 2.58 eV for the structure with two $V_{O(3)}$ and 2.91 eV for the structure with two $V_{O(4)}$.

The relative stability of $V_{O(3)}$ ¡ $V_{O(3)}$ ¡ $V_{O(4)}$ at $\Theta = \frac{1}{4}$ oxygen vacancies in (2×1) supercell remains as the cell size increases. Thus we use the (2×1) supercell expansion of CuO(111) for the further calculations. We also performed test calculations to investigate the effect of U on the Cu 3d states on the energetic preferences of the oxygen vacancies. As shown in the Fig. S1 and S2 in ESI, the energetic preference of the different oxygen vacancies at $\Theta = \frac{1}{4}$ in 1 remains irrespective of the value of U (U = 0, 3, 5.2, 7 and 9 eV). From these test calculations, we conclude that using U = 7 eV in our calculations not only yields an electronic structure consistent

with experimental, but the energetic properties are also appropriately described.

Table 1 Oxygen vacancy formation energies E_{vac} in eV for CuO(111) surface with a surface and subsurface O(3) and O(4) vacancy calculated using GGA + U and HSE06. The energetic preference decreases from left to right.

Method	$V_{O(u)}$	$V_{O(3)}$	$V_{O(d)}$	$V_{O(4)}$
GGA + U	2.68	3.02	3.52	3.52
HSE06	2.29	2.77	3.09	3.27

Fig. 3 shows the relaxed structures of CuO(111) with the O(3), O(4), O(u) and O(d) vacancy along with the stoichiometric CuO(111) surface. The corresponding changes in Bader charge for Cu are shown relative to the stoichiometric surface; changes in the charges on the O atoms are negligible. A surface Cu atom in stoichiometric CuO(111) has a computed Bader charge of 9.90 electrons. The Cu atom in Cu_2O bulk has computed Bader charge of 10.46 electrons, and hence a change in the charge of 0.5–0.6 electron is indicative of reduction from Cu^{2+} to Cu^{+}.

After relaxing the CuO(111) surface with $V_{O(3)}$, the remaining O(3) atom moves toward the vacancy site and migrates outwards, making bonds to Cu(4) atoms which also migrate toward the O(3) atom (Fig. 3(b)). The bond length Cu(4)–O(3), which was 2.73 Å before reduction, shortens by 0.7 Å. One Cu(3) and one Cu(4) atom on the surface each gains about 0.4 electrons after removal of the oxygen, indicating that in terms of formal oxidation states, these Cu^{2+} are reduced to approximately Cu^{+} in the presence of the O(3) vacancy. The surface structure with $V_{O(4)}$ is more distorted compared to the one with $V_{O(3)}$ (Fig. 3(c)). One O(3) atom is substantially shifted upward and the distance between the other O(3) and Cu(4) atoms becomes shorter. Two Cu(4) atoms move toward O(3) atoms, and the distance between Cu(4) and O(3) is shortened slightly from 1.86 Å to 1.82 Å. Two Cu(3) atoms gain 0.39 and 0.48 electrons, which we again assign as reduced Cu^{+}. From the relaxed structure of $V_{O(u)}$ (Fig. 3(d)), it is noteworthy that one of the surface O(3) atoms is significantly shifted downward. The surface Cu(3) and subsurface Cu(4) bordering the vacancy gain 0.46 and 0.47 electrons, respectively, which can be assigned as Cu^{+}. One of the O(u) atoms move toward the vacancy site in the the relaxed structure with $V_{O(d)}$ (Fig. 3(e)). While one subsurface Cu(3) atom gains 0.42 electrons, one subsurface Cu and one sub-subsurface Cu atom each gains 0.3 electron. The difference between the calculated Bader charge of these reduced Cu atoms after vacancy formation on the CuO(111) surface and a Cu^{+} ion in bulk Cu_2O is between 0.05 to 0.15 electrons, so that the assignment of these ions as Cu^{+} is reasonable. The computed spin magnetization on the reduced Cu ions is 0, consistent with formation of a Cu^{+} ion with a closed 3d shell.

Table 2 Oxygen vacancy formation energies for $\Theta = \frac{1}{2}$ relative to the existing oxygen vacancies $\Theta = \frac{1}{4}$ for CuO(111) surface calculated using using GGA + U.

Reduction path	E_{vac} (eV)
(1) $V_{O(3)} \rightarrow 2V_{O(3)}$	3.43
(2) $V_{O(3)} \rightarrow V_{O(3)} + V_{O(4)}$	1.77
(3) $V_{O(4)} \rightarrow 2V_{O(4)}$	3.01
(4) $V_{O(4)} \rightarrow V_{O(3)} + V_{O(4)}$	1.27
(5) $V_{O(u)} \rightarrow 2V_{O(u)}$	2.43
(6) $V_{O(u)} \rightarrow V_{O(u)} + V_{O(d)}$	1.74
(7) $V_{O(d)} \rightarrow 2V_{O(d)}$	2.88
(8) $V_{O(d)} \rightarrow V_{O(u)} + V_{O(d)}$	0.89
(9) $V_{O(3)} \rightarrow V_{O(3)} + V_{O(d)}$	3.38
(10) $V_{O(3)} \rightarrow V_{O(3)} + V_{O(u)}$	2.66
(11) $V_{O(4)} \rightarrow V_{O(4)} + V_{O(u)}$	2.42
(12) $V_{O(4)} \rightarrow V_{O(4)} + V_{O(d)}$	2.97

4.2 $\Theta = \frac{1}{2}$ Oxygen Vacancy

Upon removal of half of the oxygen atoms in surface/subsurface or the same number from both surface and

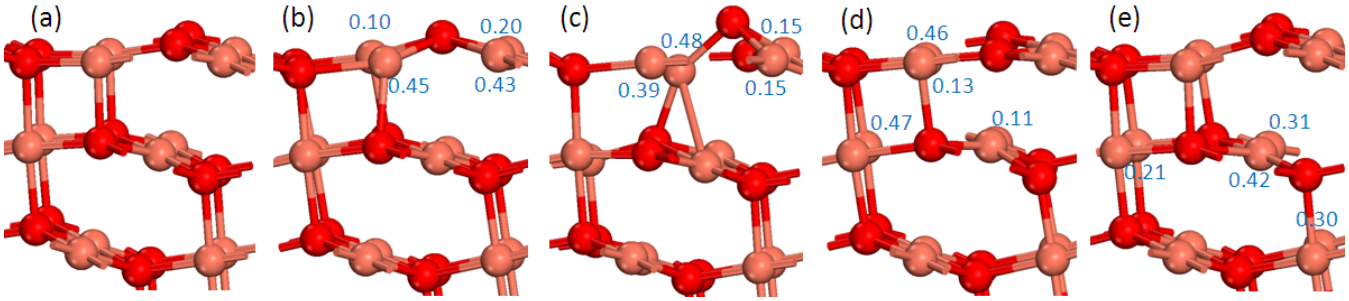

Fig. 3 Optimized structures of (2×1)–CuO(111) surface with a oxygen vacancy on the surface and subsurface. (a) stoichiometric CuO(111) (b) $V_{O(3)}$ (c) $V_{O(4)}$ (d) $V_{O(u)}$ (e) $V_{O(d)}$. Changes in Bader charge (e^-) relative to (a) are shown for Cu atoms.

subsurface, a number of different vacancy pairs can be formed in the (2×1). We can remove two O(3)/O(u) or two O(4)/O(d) atoms,or remove one O(3) and one O(4) from surface/subsurface. We can also remove one O(3) or O(4) atom from the surface and one O(u) or O(d) from subsurface. The vacancy formation energies of the vacancy pairs are computed relative to the surface with one oxygen vacancy present, and are listed in Table 2. The structure with $V_{O(u)}$ + $V_{O(d)}$, which has the formation energy E_{vac} of 1.74 eV relative to $V_{O(u)}$ and 0.89 relative to $V_{O(d)}$, is energetically most favorable compared to the other structures. The second most stable structure with a vacancy pair is the structure with $V_{O(3)}$ + $V_{O(4)}$. The $V_{O(4)}$+$V_{O(3)}$ vacancy pair can be obtained either by removing an O(3) atom from the structure with $V_{O(4)}$ ($E_{vac} =$ 1.77 eV) or by removing an O(4) atom from the structure with $V_{O(3)}$ ($E_{vac} =$ 1.27 eV). Fig. 4(a) and (b) shows these two most stable structures with an oxygen vacancy pair, along with the Cu Bader charges relative to the perfect CuO(111) surface. The combination of surface and subsurface oxygen vacancy pairs are not as energetically favourable. The less stable structures are displayed and discussed in ESI Fig. S2.

From the Bader charges shown in Fig. 4(a), it can be seen that three subsurface Cu atoms and one surface Cu atom in $V_{O(u)}$ + $V_{O(d)}$ each gains 0.4~0.6 electrons. Fig. 4(b) shows that four surface Cu atom in $V_{O(4)}$+$V_{O(3)}$ structure gains 0.4~0.7 electrons, which are close to the calculated value of the Bader charge on Cu^+ in Cu_2O bulk. The distances between the remaining O and reduced Cu atoms in the surface and subsurface are 1.84~1.89 Å, which are close to the calculated Cu–O distance of 1.85 Å in Cu_2O bulk. This shows that the four Cu^{2+} ions at and near surface are formally reduced overall to four Cu^+ ions by the presence of a vacancy pair. Furthermore, we can conclude that the reduction process $4Cu^{2+} \rightarrow 4Cu^+$ is more favourable than the competing reduction process whereby the existing Cu^+ species from the single vacancy are further reduced to Cu^0. This indicates that all the surface Cu^{2+} ions reduce to Cu^+ upon the removal of $\Theta = \frac{1}{2}$ of the oxygen atoms.

4.3 $\Theta = \frac{3}{4}$ and $\Theta = 1$ Oxygen Vacancy

Two types of triple oxygen vacancy ($\Theta = \frac{3}{4}$) can be obtained by removing of two O(3)/O(u) and one O(4)/O(d) atoms or two O(4)/O(d) and one O(3)/O(u) atoms from the surface/subsurface. The mixed surface/subsurface oxygen vacancies at $\Theta = \frac{3}{4}$ concentration are also taken into account. The most stable vacancy strcuture at $\Theta = \frac{3}{4}$ is the structure with $V_{O(u)}$ + $V_{O(d)}$ + $V_{O(3)}$, as shown in Fig. 4(c). From the rela-

tive Bader charges shown in Fig. 4(c), it can be seen that three Cu^{2+} ions in the subsurface and three surface Cu^{2+} are reduced to six Cu^{+} because each of them gain electrons around 0.5 ~0.6. The second most stable oxygen vacancy configurations at $\Theta = \frac{3}{4}$ is the structure with $V_{O(u)}$ + $2V_{O(d)}$ (See Fig. 4(d)). Four Cu^{2+} ions in the subsurface layer around the vacancies gain 0.6 ~0.7 electrons and extend their Cu–O bond lengths to 1.84–1.93 Å. Two other Cu^{2+} ions reduced by 0.4 electron, so that overall $6Cu^{2+} \rightarrow Cu^{+}$.

It can be seen that as is the case at $\Theta = \frac{1}{4}$ and $\Theta = \frac{1}{2}$ coverages, the reduction process $Cu^{2+} \rightarrow Cu^{+}$ continues to preferred over the the reduction of existing Cu^{+} to metallic Cu^{0}. We also see that layer by layer reduction of the CuO(111) surface is not favoured during the vacuum annealing since the structure with a mixture of surface and subsurface vacancies is more favorable than a configuration with $\Theta = \frac{3}{4}$ vacancies in a single layer. Energetically less favorable oxygen vacancy configurations at $\Theta = \frac{3}{4}$ have also been studied (see ESI Fig. S3).

Upon further removal of the oxygen atoms from the surface or subsurface, a coverage of oxygen vacancies equivalent to a full layer ($\Theta = 1$) is reached. The mixture of surface/subsurface can be obtained by removing three from the subsurface and one from the surface, or removing two from each of the surface and the subsurface. Fig. 4(e) and (f) shows the first and second most energetically preferred configurations at the vacancy concentration $\Theta = 1$. The most stable structure has $V_{O(u)}$ + $2V_{O(d)}$ + $V_{O(3)}$. All eight Cu^{2+} ions per cell in the surface and subsurface are reduced to the Cu^{+} due to the gain in net Bader charge of 0.5 to 0.6 electrons. The second most stable structure is the combination of two of the

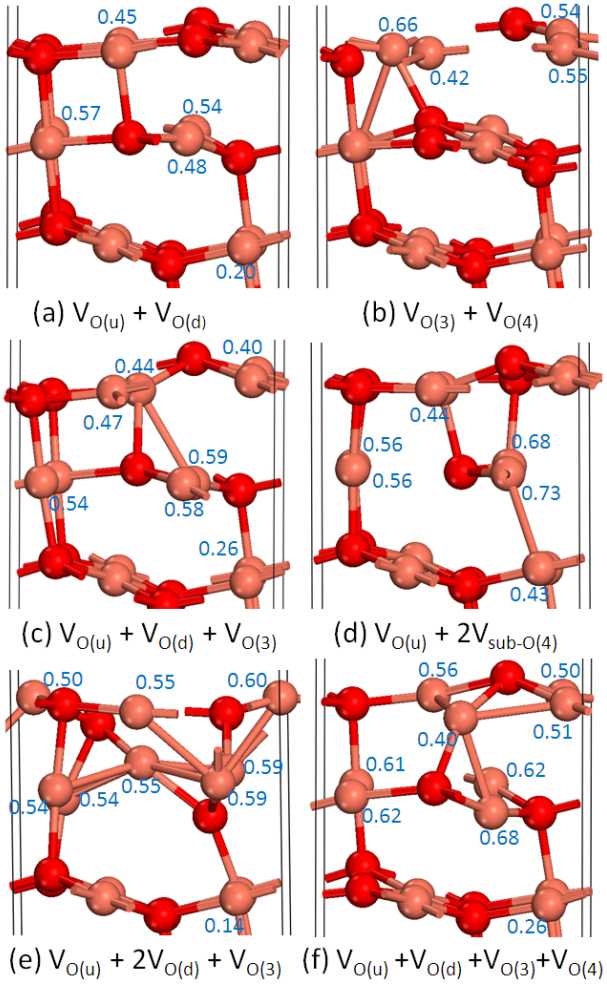

Fig. 4 Optimized structures of (2×1)–CuO(111) surface with different oxygen vacancy coverage. Changes in Bader charge (e^{-}) relative to (a) in Fig. 3 are shown for Cu atoms. (a) and (b) for $\Theta = \frac{1}{2}$, (c) and (d) for $\Theta = \frac{3}{4}$, (e) and (f) for $\Theta = 1$.

most favorable oxygen vacancies at $\Theta = \frac{1}{2}$, *e.g.* $V_{O(u)}$ + $V_{O(d)}$ + $V_{O(3)}$ + $V_{O(4)}$. In this case, all the Cu^{2+} ions have gained around 0.5~0.7 electrons, indicating that all the Cu^{2+} ions are now reduced to Cu^{+} ions. Although the complete reduction of the surface layer Cu^{2+} to metallic Cu^{0} is possible, the calculation shows that the $2V_{O(3)}$ + $2V_{O(4)}$ vacancy is not energetically favourable (see ESI Fig. S4).

We conclude that the oxygen vacancy mechanism is not sufficient to describe how CuO(111) is reduced to metallic Cu,

because the reduction process of $Cu^{2+} \rightarrow Cu^{+}$ is energetically preferred over the reduction of Cu^{+} to metallic Cu^{0}. We therefore suppose that Cu^{0} can only be formed when the diffusion of oxygen to the surface is kinetically limited, or when the entire sample has transformed into Cu_2O.

In conclusion, subsurface oxygen vacancy $V_{O(u)}$ is found to be energetically more favoured than three coordinated oxygen vacancy $V_{O(3)}$ at $\Theta = \frac{1}{4}$. The oxygen vacany pair $V_{O(u)} + V_{O(u)}$ is found to be the most stable structure at $\Theta = \frac{1}{2}$. The mixture of surface and subsurface oxygen vacancies are energetically preferred over the structures with a fully reduced monolayer at $\Theta = \frac{3}{4}$ and $\Theta = 1$. our analysis of step-wise oxygen vacancy formation can explain how the CuO(111) surface is reduced. The energetics of oxygen vacancy formation are such that at the temperatures in the experiments of ref 30, oxygen vacancy formation will take place and our results show that in all oxygen vacancy coverages, $Cu^{2+} \rightarrow Cu^{+}$ is energetically preferred over $Cu^{+} \rightarrow Cu^{0}$, and therefore Cu_2O is an intermediate state prior to it is fully reduced to metallic Cu^{0}.

4.4 Ab initio atomistic thermodynamics of oxygen vacancies on CuO(111) surface

In order to estimate the temperature for the oxygen vacancy formation on the CuO(111) surface, *ab initio* atomistic thermodynamics is used to calculate the surface free energy γ. Using eq. (6) and eq. (7), we calculate the surface free energy $\gamma(T,P)$ of the CuO(111) surface for different oxygen vacancy coverages as a function of the O atomic chemical potential (Fig. 5). The dependence of the oxygen chemical potential is translated into a temperature scale at an oxygen pressure of $P = 10^{-8}$ Torr (which would be a typical vacuum pressure in experimental work) using the standard thermodynamic tables.[34]

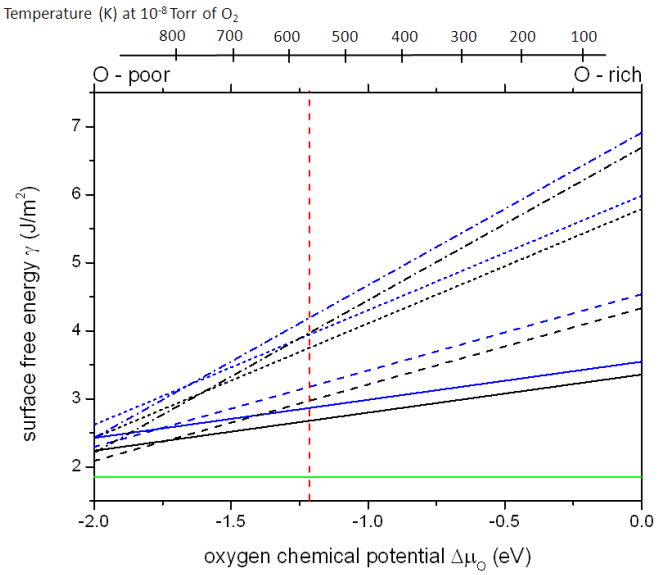

Fig. 5 Surface free energy $\gamma(T, P = 10^{-8}$ Torr) of CuO(111) surfaces with different oxygen vacancy coverage as a function of oxygen chemical potential relative to $\frac{1}{2}E(O_2)$. Solid lines are for 25 % of oxygen vacancy coverage; black line: $V_{O(u)}$, blue line: $V_{O(3)}$. Dash lines are for 50 % oxygen vacancy, black: $V_{O(u)}+V_{O(d)}$, blue: $V_{O(3)}+V_{O(4)}$. Short dashed lines are for 75 % oxygen vacancy; black: $V_{O(u)}+V_{O(d)}+V_{O(3)}$ and blue: $V_{O(u)}+2V_{O(d)}$. Dash dot lines are for 100 % oxygen vacancy; black: $V_{O(u)}+2V_{O(d)}+V_{O(3)}$ and blue: $V_{O(u)}+V_{O(d)} + V_{O(3)} + V_{O(4)}$. Green dash line is for stoichiometric CuO(111) surface. Vertical red dashed line shows the chemical potential of oxygen in Cu_2O.

From Fig. 5 we can see that the surface free energy γ increases significantly with an increase of oxygen vacancy concentration and that the stoichiometric surface is energetically favorable even under oxygen–poor conditions. This means that the reduction process is not spontaneous and that stronger reducing conditions than vacuum annealing are needed. Notice that the $\Theta = \frac{1}{2}$ oxygen vacancy structure $V_{O(u)}+V_{O(d)}$ is relatively low in energy and becomes more stable than $V_{O(u)}$ under oxygen–poor condition. This implies that Cu_2O is intermediate state during the reduction process, and CuO may reduce to Cu_2O before it is directly reduced to metallic Cu.

Thus we also calculated the formation energy of Cu_2O using

the definition $h_{Cu_2O} = \mu_{Cu_2O} - 2\mu_{Cu} - \mu_O$, where μ_{Cu_2O} is the energy of bulk Cu_2O. The calculation gives $h_{Cu_2O} = -1.24$ eV, which is very close to the previous calculation.[35] From the calculated formation energy of bulk Cu_2O, we derive a temperature of about 540 K ($P = 10^{-8}$ Torr) for the conversion of CuO into Cu_2O (shown with vertical dashed line in Fig. 5). Lee *et al.* reported the reduction of CuO to Cu_2O at 473 K and reduction of CuO to metallic Cu at 673 K through vacuum annealing at a pressure of 10^{-8} Torr.[30] Our calculated result is consistent with the experimentally measured conditions under which CuO is reduced to Cu_2O. An error bar for the temperature in the range of 100–200 K is due to the translation of an uncertainty of the vacancy formation energy of a few tenths of an eV from the DFT calculations.[36]

5 Reduction of the CuO(111) surface with H_2

Reduction of transition metal oxides with H_2 has been used to grow thin metallic films. In this section, we study the reaction of H_2 with the CuO(111) surface as a model of the initial stages in H_2 reduction of CuO. Since accommodating four H_2 molecules per (2×1) cell simultaneously at the surface is not favourable, we focus on the more reasonable route of sequential adsorption of H_2 on the CuO(111) surface, until a full layer of surface oxygen is removed.

5.1 Sequential adsorption of H_2 on CuO(111) surface

For the first H_2 molecule, there are two different adsorption sites, O(4) and O(3). The calculated adsorption energy ΔE_{ads} of H_2 on O(4) is 0.02 eV, which indicates that there is no reaction of H_2 on the O(4) site. However, the adsorption of H_2 on the O(3) site is quite exothermic with a gain of ΔE_{ads} =-0.82 eV at T = 0 K. Consistent with our oxygen vacancy calculation, this is because O(3) is more reactive than O(4) (sect. 4). The relaxed atomic structure of H_2 on the O(3) site is shown in Fig. 6(a). Oxygen O(3) is pulled out of the surface upon reaction with H_2 to form a water molecule. The distance between this oxygen atom and H is about 1.0 Å and the angle H–O–H is 107.5°, typical of the water molecule. The distance between the O atom in the water molecule and the nearest Cu is 1.99 Å, which is notably longer than the Cu–O distance in the CuO(111) surface layer. The desorption energy of the formed water molecule from the surface is ΔE_{des} = 0.78 eV. If the desorption energy is positive, additional thermal energy is needed to break the bond between O in H_2O and the surface Cu atom. Thus, the dissociative adsorption of a H_2 molecule on the O(3) site on CuO(111) leads to spontaneous formation of a water molecule and partial reduction of the CuO (111) surface. However desorption of water from the surface is not spontaneous at T = 0 K, and elevated temperature is needed to desorb water. Bader charge analysis of H_2 adsorption on the O(3) site shows that one Cu(3) and one Cu(4) atom on the surface gain 0.43 and 0.23 electrons, respectively, indicating that H_2 adsorption on the CuO(111) surface can reduce two Cu^{2+} ions to Cu^+, which is consistent with the reduction process observed in sect. 4.1 for oxygen vacancy formation.

The next H_2 adsorption on the partially reduced CuO(111) surface with 25 % oxygen vacancy takes place after removing the formed H_2O molecule. The calculated adsorption energy ΔE_{ads} of this H_2 molecule on the remaining O(3) is -0.40 eV (Fig. 6(b)). The angle H–O–H is 106.6° and the H–O distance is 0.98 Å. The distance between O in water and the nearest surface Cu is 2.00 Å. This indicates that another water molecule

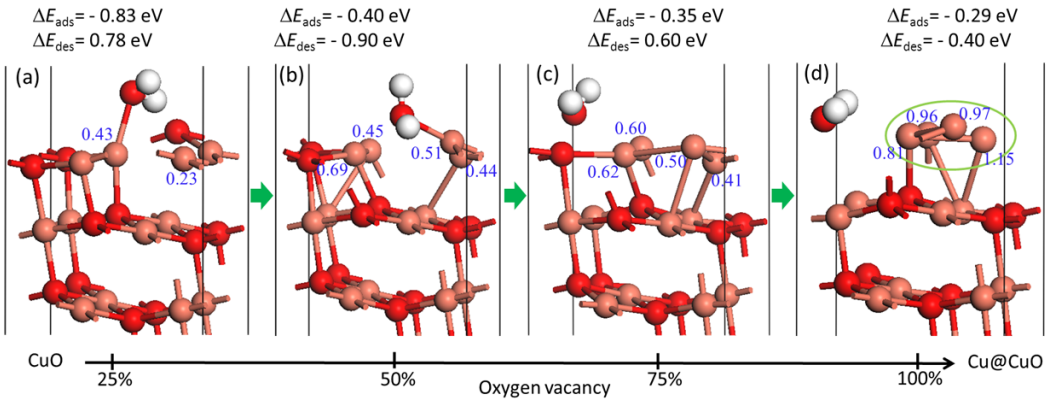

Fig. 6 Structure of the CuO(111) surface after adsorption of each H_2 molecule and formation of water, The adsorption energy of H_2 on the surface (ΔE_{ads}) and desorption energy of water from the surface (ΔE_{des}) are shown on the top of each subfigure. The arrows in green represent the removal of formed water molecule and introducing another H_2 on the partially reduced surface. The arrow in the bottom indicates the trend of reduction. Changes in Bader charge (e^-) relative to Fig. 4(a) are shown for Cu atoms in the top layer.

formed spontaneously on the partially reduced surface. The change in Bader charge on surface Cu is shown in Fig 6(b). Two Cu(4) atoms gain 0.65 and 0.40 electrons and the other two Cu(3) atoms gain 0.51 and 0.44 electrons after the second H_2 is introduced to the surface, indicating further reduction of Cu. The Cu–O distance is shortened from 1.95 Å to 1.84 Å for each of Cu(3) and Cu(4) atoms. This implies that all the Cu^{2+} are reduced to Cu^+. At this point we can conclude that the $Cu^{2+} \rightarrow Cu^+$ process is spontaneous in the presence of reducing agent H_2. In this case, the desorption energy ΔE_{des} is negative, and no thermal effect is needed to remove the water molecule from the surface.

The O(4) atoms on the stoichiometric CuO(111) surface are initially not reactive to H_2 molecule. However, The third H_2 molecule reacts with an O(4) atom at the surface with two $V_{O(3)}$ because it is shifted upward and Cu - O(3) bond is weakened. (Fig. 6(c)). This indicates that the reactivity of the CuO(111) surface increases with the presence of oxygen vacancies. A water molecule is formed with an adsorption energy of ΔE_{ads}= -0.35 eV, which is weaker compared to adsorption on O(3) because O(4) has a higher coordination number and is less favourable to remove. The desorption of water molecule is not favoured in this case because the desorption energy is positive. The distance between the O in H_2O molecule and the Cu atom is 3.09 Å. The H –O distances in H_2O are 0.98 and 0.99 Å, and the H –O –H angle is 109.6°. The Cu(4) atoms gain 0.60 and 0.62 electrons, while other Cu(3) atoms gain 0.41 and 0.50 electrons, respectively. The distance between the Cu(4) that gains 0.62 electron and O(3) is 2.61 Å, which is very close to bulk Cu–Cu distance. The Cu–O distance on the surface is about 1.84 to 1.90 Å. From the above Bader charge and the structure analysis, we conclude that metallic copper species are formed at this coverage of 75 % oxygen vacancies, and other Cu^{2+} ions are reduced to Cu^+, so that Cu^0 and Cu^+ co-exist on this surface.

Finally, the interaction of H_2 with the last surface oxygen atom O(4) which is shifted upward by the adsorption of previous H_2 gives formation of a water molecule with an adsorption energy of -0.29 eV (Fig. 6(d)). It is of note that the H_2 adsorption energies ΔE_{ads} on the CuO(111) surface with dif-

ferent oxygen vacancies are all negative, which shows that the reduction of the surface is energetically favoured. The Cu–Cu distance on the surface is in the range of 2.4 to 2.8 Å, compared to 2.55 Å in bulk Cu metal. The change in the Bader charge on Cu surface atoms in Fig. 6(d) indicates that full reduction of the surface Cu^{2+} ions to metallic Cu takes place. From the Bader charges shown in Fig. 6, we can conclude that indirect reduction of CuO→Cu_2O →Cu is again dominant over direct reduction CuO→Cu, which is consistent with our oxygen vacancy calculations and the experimental results.[38]

5.2 Ab initio atomistic thermodynamics of H_2 adsorption on CuO(111) surface

To understand the structural stability and effect of temperature during the reduction of the CuO (111) surface with H_2, we again apply *ab initio* thermodynamics using eq. (6) and eq. (7). Fig. 7 shows the surface free energy γ of CuO(111) surfaces with the different percentage of oxygen vacancies for each sequential adsorption of H_2 as a function of oxygen chemical potential μ_O at 1 bar of O_2 pressure. By drawing a vertical line through the point where the horizontal black dashed line (stoichiometric CuO(111) surface) and the red line (50 % vacancies) cross, we know that Cu^{2+} ions on the CuO(111) surface start reducing to Cu^+ at circa 360 K. This process continues until the temperature goes up to 780 K where the green line (100 % reduced CuO(111) surface) crosses the red line. Therefore a Cu_2O to metallic copper transition occurs at this point, and metallic Cu islands form on CuO, as highlighted in Fig. 6(d). Rodriguez *et al.* observed the reduction of CuO to Cu_2O with low H_2 flow at atmospheric H_2 pressure and elevated temperature 423–673 K using *in situ* time-resolved XRD technique,[37] which is consistent with Fig. 7.

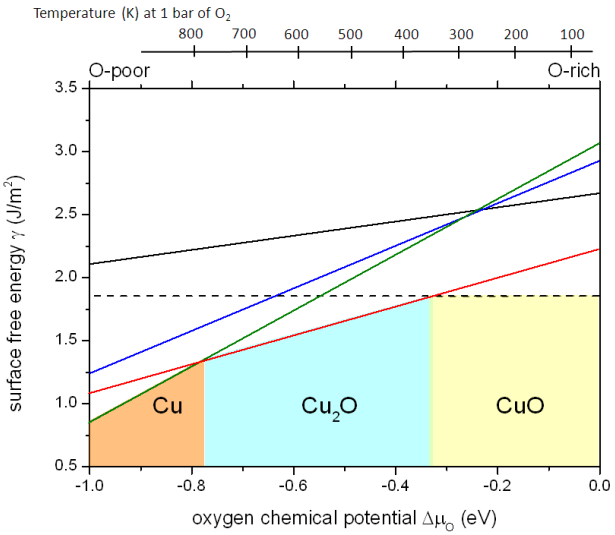

Fig. 7 Surface free energy γ of CuO(111) surfaces with different oxygen vacancies in the presence of H_2 as the function of oxygen chemical potential $\Delta\mu_O$. black: 25 %, red: 50 %, blue: 75 %, green: 100 %. black dashed line: stoichiometric CuO(111) surface.

By juxtaposing Fig. 5 with Fig. 7 which are both obtained from *ab initio* atomistic thermodynamics studies, one should notice that Fig. 7 corresponds to the continuation of the left-hand-side of Fig. 5 because the O–poor condition in reduction of the surface with oxygen vacancy is the O–rich condition for the reduction of the surface with H_2 adsorption. It can be seen that the lines with the same percentage of oxygen vacancies are parallel in these two figures. The surface free energies γ in Fig. 5 increase if the pressure increases. Thus we can compare these two figures and can come to the conclusion that reduction of the CuO(111) surface to metallic Cu is energetically difficult to achieve without a reducing agent because all the lines in Fig. 7 in general lie below the lines in Fig. 5. The horizontal line in Fig. 5, which corresponds to the stoichiometric CuO(111) surface, lies under all the other lines, even at the oxygen-poor condition. However in Fig. 7, this line is crossed by the red line (50 % O vacancies) at $\Delta\mu_O = -0.33$ eV and by

the green line (100 % O vacancies) at $\Delta\mu_O = -0.77$ eV. This indicates that the CuO(111) surface can be reduced by H_2 to Cu_2O and finally to metallic Cu. It should also be noticed that the extreme left-hand-side of Fig. 7 corresponds to the reduction energies of CuO(111) with H_2 which are calculated using eq. 4 and are in line with the data in Fig. 6.

Combining the ideas of Fig. 5 and Fig. 7, we obtain a schematic phase diagram for the reduction of CuO(111) surface to metallic Cu with and without H_2 reducing agent, as shown in Fig. 8. The vertical dashed red lines approximately show the formation energies of the bulk Cu_2O and CuO by which the H_2 pressures are obtained. Fig. 5 corresponds to the reduction of the bulk phase CuO because the Cu and the CuO bulk energies are used to obtain the lower and higher limit of oxygen chemical potential μ_O. The range of oxygen chemical potential μ_O in Fig. 7 is derived from the reduction condition where the CuO(111) surface is reduced with H_2. We have found surface structures that corresponds to the mixtures of oxidation states expected under the same conditions in the bulk, namely, Cu^{2+} and Cu^{+} at 25 % vacancy coverages and Cu^{+} and Cu^{0} at 75 %. However, as shown in Fig. 5, these are not as stable at the surface under these conditions as stoichiometric CuO. The mixtures of these oxidation states at 25 % and 75 % oxygen vacancies are not preferred during the reduction of CuO with H_2 in Fig. 7. This is summarized in Fig. 8. Fig. 8 shows that different processes are needed for bulk and surface reduction, *i.e.* reducing the O_2 pressure is adequate for bulk reduction, but applying H_2 is needed for surface reduction. From Fig. 8, we can see that the bulk CuO is reduced to the mixture of CuO and Cu_2O as the oxygen pressure decreases, then to the the mixture of Cu_2O and Cu^0 near vacuum region. The surface CuO needs a stronger reduction condition compared to the reduction of bulk CuO. The surface CuO transforms to Cu_2O with the application of H_2 and eventually to metallic Cu with increased H_2 pressure. This implies that the surface oxides protect the underlying bulk from reduction during vacuum annealing. Applying the reducing agent H_2 can significantly facilitate the reduction of CuO.

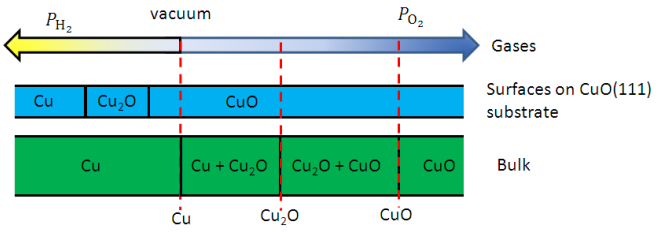

Fig. 8 Schematic phase diagram of CuO(111) reduction to metallic Cu under different oxygen and H_2 pressures. green and blue colours represent bulk and surface, respectively.

6 Conclusions

In conclusion, we studied two mechanisms for the reduction of CuO(111) surface, namely oxygen vacancies from vacuum annealing and H_2 adsorption. Oxygen vacancy calculations reveal that removal of under-coordinated O(u) atom is energetically more favourable than removal of four-fold O(3). The mixture of surface/subsurface vacancy is found to more favourable than a single layer oxygen vacancies at $\Theta = \frac{3}{4}$ and =1. The reduction process $Cu^{2+} \rightarrow Cu^{+}$ is found to be more favoured than the process $Cu^{+} \rightarrow Cu^{0}$ at all the vacancy concentrations, indicating that vacuum annealing is not sufficient during the indirect ALD. The calculation of sequential adsorption of H_2 on the CuO(111) surface shows that H_2 adsorption initially takes place on the O(3) site, giving a water molecule and the partially reduced surface. Subsequent adsorption of

H_2 fully reduces the surface and gives water molecules. Comparing the results from *ab initio* atomistic thermodynamics for the two mechanisms, we conclude that the reduction of the CuO surface with H_2 is more favoured over the reduction through vacuum annealing. For indirect ALD processes, these results show that the the role of reducing agent is important to obtain fully reduced metal thin films.

Acknowledgments

We acknowledge support from Science Foundation Ireland (SFI) under the 'ALDesign' Project (grant number 09.IN1.I2628). MN acknowledges support from Science Foundation Ireland through the Starting Investigator Research Grant Program (EMOIN (SIRG/09/I1620)). We acknowledge the SFI and Higher Education Authority funded Irish Centre for High Performance Computing (ICHEC) for access and SFI funded computational resources at the Tyndall National Institute.

References

1 C. S. Hau-Riege, *Microelectronics Reliability*, 2004, **44**, 195–205.

2 R. Rosenberg, D. C. Edelstein, C.-K. Hu and K. P. Rodbell, *Annual Review of Materials Science*, 2000, **30**, 229–262.

3 Y. Shacham-Diamand, A. Inberg, Y. Sverdlov, V. Bogush, N. Croitoru, H. Moscovich and A. Freeman, *Electrochimica Acta*, 2003, **48**, 2987 – 2996.

4 V. Krisyuk, L. Aloui, N. Prud'homme, S. Sysoev, F. Senocq, D. Samélor and C. Vahlas, *Electrochemical and Solid-State Letters*, 2011, **14**, D26–D29.

5 B. H. Lee, J. K. Hwang, J. W. Nam, S. U. Lee, J. T. Kim, S.-M. Koo, A. Baunemann, R. A. Fischer and M. M. Sung, *Angewandte Chemie International Edition*, 2009, **48**, 4536–4539.

6 B. Vidjayacoumar, D. J. H. Emslie, S. B. Clendenning, J. M. Blackwell, J. F. Britten and A. Rheingold, *Chemistry of Materials*, 2010, **22**, 4844–4853.

7 Lim Booyong S., Rahtu Antti and Gordon Roy G., *Nat Mater*, 2003, **2**, 749–754.

8 S. M. George, *Chemical Reviews*, 2010, **110**, 111–131.

9 V. Miikkulainen, M. Leskela, M. Ritala and R. L. Puurunen, *Journal of Applied Physics*, 2013, **113**, 021301.

10 M. Utriainen, M. Kröger-Laukkanen, L.-S. Johansson and L. Niinistö, *Applied Surface Science*, 2000, **157**, 151 – 158.

11 Z. Li and R. G. Gordon, *Chemical Vapor Deposition*, 2006, **12**, 435–441.

12 T. J. Knisley, T. C. Ariyasena, T. Sajavaara, M. J. Saly and C. H. Winter, *Chemistry of Materials*, 2011, **23**, 4417–4419.

13 J. Chae, H.-S. Park and S.-w. Kang, *Electrochemical and Solid-State Letters*, 2002, **5**, C64–C66.

14 J. Hamalainen, T. Hatanpaa, E. Puukilainen, T. Sajavaara, M. Ritala and M. Leskela, *J. Mater. Chem.*, 2011, **21**, 16488–16493.

15 G. Kresse and J. Hafner, *Phys. Rev. B*, 1994, **49**, 14251–14269.

16 G. Kresse and J. Furthmüller, *Computational Materials Science*, 1996, **6**, 15 – 50.

17 J. P. Perdew, K. Burke and M. Ernzerhof, *Phys. Rev. Lett.*, 1997, **78**, 1396–1396.

18 L. Wang, T. Maxisch and G. Ceder, *Phys. Rev. B*, 2006, **73**, 195107.

19 S. L. Dudarev, G. A. Botton, S. Y. Savrasov, C. J. Humphreys and A. P. Sutton, *Phys. Rev. B*, 1998, **57**, 1505–1509.

20 M. Nolan and S. D. Elliott, *Phys. Chem. Chem. Phys.*, 2006, **8**, 5350–5358.

21 J. Heyd, G. E. Scuseria and M. Ernzerhof, *The Journal of Chemical Physics*, 2003, **118**, year.

22 J. Heyd and G. E. Scuseria, *The Journal of Chemical Physics*, 2004, **121**, year.

23 D. Lide, *CRC handbook of chemistry and physics 79th edition*, Taylor & Francis, 1998.

24 M. V. Ganduglia-Pirovano, J. L. F. Da Silva and J. Sauer, *Phys. Rev. Lett.*, 2009, **102**, 026101.

25 K. Reuter and M. Scheffler, *Phys. Rev. B*, 2001, **65**, 035406.

26 S. Åsbrink and L.-J. Norrby, *Acta Crystallographica Section B*, 1970, **26**, 8–15.

27 F. Marabelli, G. B. Parravicini and F. Salghetti-Drioli, *Phys. Rev. B*, 1995,

52, 1433–1436.

28 J. Hu, D. Li, J. G. Lu and R. Wu, *The Journal of Physical Chemistry C*, 2010, **114**, 17120–17126.

29 B. X. Yang, T. R. Thurston, J. M. Tranquada and G. Shirane, *Phys. Rev. B*, 1989, **39**, 4343–4349.

30 S. Lee, N. Mettlach, N. Nguyen, Y. Sun and J. White, *Applied Surface Science*, 2003, **206**, 102 – 109.

31 G. Henkelman, A. Arnaldsson and H. Jónsson, *Computational Materials Science*, 2006, **36**, 354 – 360.

32 M. V. Ganduglia-Pirovano, A. Hofmann and J. Sauer, *Surface Science Reports*, 2007, **62**, 219 – 270.

33 B. J. Morgan and G. W. Watson, *The Journal of Physical Chemistry C*, 2009, **113**, 7322–7328.

34 D. R. P. H. Stull, *JANAF thermochemical tables*, U.S. Dept. of Commerce, National Bureau of Standards, Washington, D.C., 2nd edn, 1971.

35 C. Li, F. Wang, S. Li, Q. Sun and Y. Jia, *Physics Letters A*, 2010, **374**, 2994 – 2998.

36 P. M. Kowalski, B. Meyer and D. Marx, *Phys. Rev. B*, 2009, **79**, 115410.

37 J. Rodriguez, J. Kim, J. Hanson, M. Pérez and A. Frenkel, *Catalysis Letters*, 2003, **85**, year.

38 J. Y. Kim, J. A. Rodriguez, J. C. Hanson, A. I. Frenkel and P. L. Lee, *Journal of the American Chemical Society*, 2003, **125**, 10684–10692.

39 J. A. A. Rodriguez, J. C. Hanson, A. I. Frenkel, J. Y. Kim and M. Pérez, *Journal of the American Chemical Society*, 2002, **124**, 346–354.